Kinetic Study of the 2-Naphthyl ($C_{10}H_7$) Radical Reaction with C_2H_2

J. Park,* Hue M. T. Nguyen,† Z. F. Xu, and M. C. Lin*

Department of Chemistry, Emory University, Atlanta, Georgia 30322

Received: June 22, 2009; Revised Manuscript Received: August 18, 2009

The kinetics for the gas-phase reaction of 2-naphthyl radical with acetylene has been measured by monitoring the $C_{10}H_7O_2$ radical in the visible region employing cavity ringdown spectrometry (CRDS) using 2-$C_{10}H_7Br$ as a radical source photolyzing at 193 nm in the presence of a small fixed amount of O_2 at 40 Torr pressure with Ar as a diluent. Absolute rate constants measured at temperatures between 303 and 448 K can be expressed by the following Arrhenius equation: $k(T) = (3.36 \pm 0.63) \times 10^{11} \exp[-(817 \pm 34)/T]$ cm^3 mol^{-1} s^{-1}. Theoretically, the potential energy surfaces (PESs) for the reactions of acetylene with 1- and 2-$C_{10}H_7$ radicals have been calculated with the G2MS//B3LYP/6-311+G(d,p) method. The PESs show that the reactions of 1- and 2-$C_{10}H_7$ with C_2H_2 occur first by forming adducts with 2.6 and 2.9 kcal/mol barriers, respectively. The rate constants for the stabilization and decomposition of the adducts have been predicted by RRKM/ME calculations. The mechanisms for the decomposition of the two adducts were predicted to be distinctively different under experimental conditions; the excited 1-$C_{10}H_7C_2H_2$ radical produces primarily acenaphthylene because of its low formation barrier, while the excited 2-$C_{10}H_7C_2H_2$ radical can be effectively stabilized by collisional quenching due to its high exit barrier. The predicted rate constant for the 2-$C_{10}H_7$ reaction with C_2H_2 is in reasonable agreement with the experimental values under the conditions employed.

Introduction

Better understanding of the mechanisms responsible for the formation of polycyclic aromatic hydrocarbons (PAHs), which are known to be directly relevant to the formation of soot, has been one of the most important and challenging problems in hydrocarbon combustion. As small aromatic radicals such as phenyl (C_6H_5), phenylvinyl ($C_6H_5C_2H_2$), naphthyl ($C_{10}H_7$), and their derivatives are believed to play a pivotal role in the formation of naphthalene ($C_{10}H_8$) by HACA (H-abstraction, C_2H_2-addition) reactions and cyclization reactions, namely

$$C_6H_5 + C_2H_2 \rightarrow C_6H_5C_2H_2$$

$$C_6H_5C_2H_2 + C_2H_2 \rightarrow C_6H_5C_4H_4 \rightarrow C_{10}H_8 + H$$

The repetition of such a successive abstraction/addition/cyclization process involving increasingly larger aromatic radicals has been proposed as a possible route to the formation of PAHs which give rise to soot.[1−3] Therefore, naphthyl radicals (see below) play a very significant role in the formation of larger PAHs during the incipient soot formation stages.[4,5]

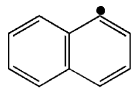

1-$C_{10}H_7$

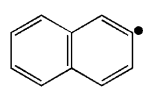

2-$C_{10}H_7$

In 1994, Wang and Frenklach[6] investigated theoretically the reaction of acetylene with a series of one- and multiring aromatic radicals by semiempirical quantum mechanical AM1 calculations, in which the addition of C_2H_2 to 1-$C_{10}H_7$ was studied including association, isomerization, and H-elimination leading to acenaphthylene. They predicted the rate constants at 300−2500 K and at different pressures by TST/RRKM theory with the solution of master equation. The result showed that the high-pressure-limit rate constants for C_2H_2 addition to phenyl, 2-ethynylphenyl, and 1-naphthyl radicals were not affected by the aromatic radical size, but the molecular size did affect the distribution of product channels largely due to the increased collisional stabilization efficiency as the adduct size increased. In 2000 and 2001, Richter and co-workers[4,5] obtained more reaction channels for C_2H_2 + 1-$C_{10}H_7$ at the B3LYP/cc-pVDZ level of theory. The rate constants of the C_2H_2 + 1-$C_{10}H_7$ system were calculated by employing the TST/QRRK theory at 300−2100 K and 20 Torr−10 atm. More recently, Kislov and his co-workers[7] calculated the reaction pathway from 1-naphthyl + C_2H_2 to acenaphthalene at the G3(MP2,CC)//B3LPY/6-311G(d,p) level of theory, and the rate constants for individual reaction steps were also computed using Transition State Theory (TST) calculations at the high-pressure limit. However, no experimental kinetic data are available for $C_6H_5C_2H_2$ and $C_{10}H_7$ radical reactions of interest to combustion. In the past few years, we have carried out extensive kinetic measurements for C_6H_5 radical reactions by means of three complementary kinetic techniques, pulsed laser photolysis/mass spectrometry (PLP/MS), cavity ringdown spectrometer (CRDS), and pyrolysis/FTIR spectrometry (P/FTIRS). However, it is not yet clear if our phenyl kinetic data can be directly employed for modeling of reactions of naphthyl and bigger aryl radicals for soot growth. Similarly, the effect of phenyl substitution in the vinyl radical on its kinetics is also unknown. For example, what is the relative rate of C_2H_2 reactions with vinyl and phenylvinyl radicals? In our recent work,[8] we compared the rate constants for O_2 reactions with C_6H_5, $C_6H_5C_2H_2$, and 2-$C_{10}H_7$ radicals. From phenyl to phenylvinyl reactions, the rate constants were found

* To whom correspondence should be addressed. E-mail: jpark05@emory.edu (J.P.); chemmcl@emory.edu (M.C.L.).

† Emerson Center visiting fellow. Permanent address: Faculty of Chemistry and Center for Computational Science, Hanoi National University of Education, Hanoi, Vietnam.

10.1021/jp905854c CCC: $40.75
Published on Web 10/01/2009

to be reduced by a factor of 3−5 between 300 and 400 K, and that of the 2-$C_{10}H_7$ reaction is about 2 times slower than that of the analogous $C_6H_5 + O_2$ reaction. Clearly, there is a need to acquire more kinetic data for bigger aromatic radical reactions beyond phenyl; the results of the three radical reactions with O_2 as alluded to above indicate the significantly different reactivities of these radicals despite the fact that they are all barrierless association reactions. Comparison of the measured rate constant for $C_{10}H_7 + C_2H_2$ with that of $C_6H_5 + C_2H_2$ should provide a valuable piece of information on the potential change in the reactivity with the size/number of aromatic rings, a critical datum which is still missing for soot formation modeling. Additional reliable kinetic data for phenylvinyl and naphthyl reactions are essential for calibration and establishment of a reliable computational protocol for prediction of larger aryl radical reactions which cannot be readily studied experimentally.

In this study, we investigated the effect of temperature on the $C_{10}H_7$ reaction with C_2H_2 by CRDS using 2-$C_{10}H_7Br$ as a radical source by photolysis at 193 nm. The kinetics was determined by monitoring the change in the $C_{10}H_7O_2$ yields (or signals) as a function of C_2H_2 concentration using a mixture containing the radical precursor and a small fixed amount of O_2 as we have employed in our earlier study of the $C_6H_5 + CCl_4$ kinetics by probing the time-resolved CRDS signal of $C_6H_5O_2$ using a reaction mixture containing C_6H_5NO, CCl_4, and a small amount of O_2.[9] In this study, the results obtained by monitoring both $C_6H_5O_2$ and C_6H_5 were found to agree quantitatively with each other. In the present work, the observed kinetic data and associated mechanism have also been interpreted with quantum chemical calculations. Since most experimental measurements for large radicals are limited to low temperature (<1000 K) and pressure (<1 atm) due to probing constraints, these data may not be directly applied to typical combustion conditions where soot begins to form, and its mechanism is dramatically changed and typically very complex. Therefore, the combination of experimental and theoretical studies is not only crucial to our understanding of the mechanism but also helpful for prediction and extrapolation of low-temperature rate constants to much higher temperature and pressure regimes of interest to combustion.

Experimental Methodologies

Kinetic measurements for the 2-$C_{10}H_7 + C_2H_2$ reaction were performed by monitoring $C_{10}H_7O_2$ with CRDS under slow-flow conditions using Ar as a carrier gas at the total pressure of 40 Torr in the temperature range of 303−448 K. The experimental system used in this study consists of a heatable 50 cm long Pyrex flow tube, two lasers for radical generation and its detection, and a data acquisition system. The reactor was vacuum-sealed at the ends with a pair of highly reflective mirrors ($R = 0.9999$ at 500 nm; radius curvature, 6 m), which form a high-quality optical cavity, approximately 50 cm in length. The quality of the cavity is such that a pulse of a probing dye laser operating at 500 nm with fwhm ≃ 10 ns can be lengthened to about 45 μs. The mixing of the reactants was controlled by calibrated mass flow controllers (MKS 0258C). A constant reaction pressure was monitored by a MKS Baratron manometer. The temperature in the reactor was maintained within ±0.7 K and measured with a calibrated K-type (Alumel−Chromel) thermocouple located below the center of the probing region.

Two pulsed lasers were employed, one for the generation of the $C_{10}H_7$ radical employing a Lambda Physik Compex 105 excimer laser at 193 nm (with 2-$C_{10}H_7Br$ as the radical precursor) and the other for the detection of $C_{10}H_7O_2$ employing a Lambda Physik excimer laser (EMG201) pumped tunable dye laser (FL3002). It has a half-width of about 10 ns and a pulse energy of 1−2 mJ at 500 nm. A small fraction of the probing photon pulse transmitted through the second cavity mirror was directly detected by a Hamamatsu photomultiplier tube (PMT). The PMT signal was acquired and averaged by using a lock-in multichannel digital oscilloscope (LeCroy 140). Two lasers and the triggering of the data acquisition system were controlled by a pulse-delay generator (SRC DG 535) interfaced with a computer by means of the LABVIEW program. Typically, 20 pulses were collected at the rate of 2 Hz for each time delay. The averaged signal was stored in a computer for future data analysis.

The concentration of each individual molecule was obtained by the following formula: $[R] = 9.66 \times 10^{16}(\%)PF_R/TF_T$ molecules/cm^3, where % is the percentage of each molecule in its gas mixture, P is the total reaction pressure in Torr, T is the reaction temperature, F_R is the flow rate of each gas mixture, and F_T is the total flow rate of all gases. The typical resident time in the probing zone was ∼50 msec, and the repetition rate of 2 Hz allowed enough time for a fresh sample in the reactor between pulses. The effect of a slow repetition rate of 1 Hz was negligible in the transient signals. The flow rates were measured by mass flowmeters (MKS, 0258C), and the gas pressure was measured with an MKS Baratron manometer. The mole fraction of 2-$C_{10}H_7Br$ was typically <1.0%, and the conversion of 2-$C_{10}H_7Br$ was in the range of 2−5% depending on photolytic laser energy.

In kinetic measurements, the CRDS technique was employed to detect the transient concentration of a radical of interest by determining the decay times of the injected probing photons in the absence (t_0) and the presence (t_c) of the radical. The two decay times can be related with the concentration of the absorbing species inside of the cavity by eq 1

$$1/t_c = 1/t_0 + A \exp(-t/\tau) \quad (1)$$

where A is a constant containing the concentration of the absorbing species at time t and experimental parameters such as the cavity length (∼50 cm), the refractive index of the absorbing medium, and so forth; τ is the lifetime of the absorbing species inside of the cavity.[10]

2-$C_{10}H_7Br$ (Aldrich, 97%) was purified by means of the freeze−pump−thaw degassing procedure with liquid nitrogen (77 K). Ar, C_2H_2, and O_2 (Specialty Gases, 99.995% UHP grade) were used without further purification.

Computational Methods

The geometries of the reactants, products, intermediates, and transition states on the doublet electronic ground-state potential energy surfaces (PESs) of the reactions of C_2H_2 with both 1- and 2-naphthyl radicals were optimized[11,12] by the density functional theory at the B3LYP level[13,14] with the 6-311+G(d, p) basis set. All of the stationary points have been identified for local minima and transition states by vibrational analysis. Unscaled vibrational frequencies were employed for the calculation of zero-point energy (ZPE) corrections, the characterization of stationary points, and rate constant calculations. For a more accurate evaluation of the energetic parameters, higher-level single-point energy calculations of the stationary points were carried out by the modified Gaussian-2 (G2MS) theory,[15] based on the optimized geometries at the B3LYP/6-311+G(d, p) level

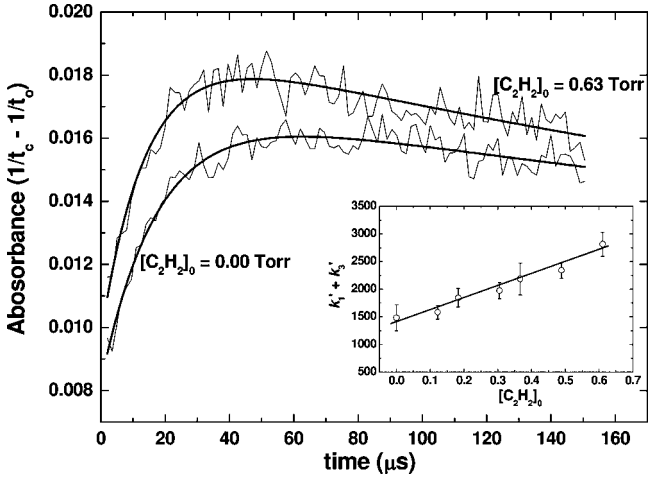

Figure 1. Typical time-resolved absorption plots of $C_{10}H_7O_2$ formed in the 2-$C_{10}H_7$ + C_2H_2 reaction at 303 K with a fixed concentration of $[O_2] = 0.16$ Torr; solid curves are fitted values using eq 2. Inset, k' versus $[C_2H_2]$ plot at 303 K.

of theory. All electronic structure calculations were performed with Gaussian 03 program.[16]

The microcanonical Rice−Ramsperger−Kassel−Marcus (RRKM) theory[17−20] was employed to calculate the rate constants of the reactions by VARIFLEX.[21] The component rates were evaluated at the *E*/*J*-resolved level, and the pressure dependence was treated by one-dimensional master equation calculations using the Boltzmann probability of the $C_{10}H_7CHCH$ adduct for the *J*-distribution. For estimating the frequency of collisions, the Lennard-Jones (L-J) parameters of Ar, ε/k_B = 114.0 K and σ = 3.47 Å, were taken from the literature,[22] while those of the adduct were approximately taken to be those of naphthalene, ε/k_B = 495 K and σ = 6.44 Å, computed at its critical temperature (747 K) and critical pressure (40.6 atm).[22,23] The averaged step size for energy transfer per collision, $\langle\Delta E\rangle_{down}$, was taken to be 300 cm^{-1} for the standard form of the "exponential down" model.[24] The maximum energy limit, E_{max} = 180 kcal/mol, was used for the energy integration in the master equation computation to ensure the convergence at high temperature.

Results and Discussion

1. Kinetic Measurements. As alluded to above, the kinetics for the 2-$C_{10}H_7$ + C_2H_2 reaction has been measured at temperatures of 303−448 K by indirectly monitoring $C_{10}H_7O_2$ with CRDS using 2-$C_{10}H_7Br$ as a radical source by photolysis at 193 nm. We selected 2-$C_{10}H_7$ in our study of the naphthyl kinetics because of the stronger extinction coefficient of 2-$C_{10}H_7Br$ than that of 1-$C_{10}H_7Br$ at 193 nm and higher radical concentrations as described in our recent work.[8] The kinetics was determined by monitoring the change in the $C_{10}H_7O_2$ yields (or signals) as a function of the concentration of C_2H_2, using a mixture containing the radical precursor with a small fixed amount of O_2. Typical time-resolved signals of the $C_{10}H_7O_2$ radical observed in this initial experiment are shown in Figure 1. The signals were analyzed for kinetic determination with the scheme

$$C_{10}H_7 + O_2 \xrightarrow{k_1} C_{10}H_7OO \xrightarrow{k_2} \text{other products}$$

$$C_{10}H_7 + C_2H_2 \xrightarrow{k_3} C_{10}H_7C_2H_2$$

The kinetic equation based on the scheme for the measured cavity photon decay times due to $C_{10}H_7O_2$ absorption in the absence (t_0) and the presence (t_c) of absorbing species at time t can be described by

$$1/t_c - 1/t_0 = B\cdot[(k_1'+k_3')/\{k_2'-(k_1'+k_3')\}]\cdot[\exp\{-(k_1'+k_3')t\} - \exp(-k_2't)] \quad (2a)$$

where k_i' is the pseudo-first-order rate coefficient of ith reaction and B contains the initial concentration of the radical species of interest and experimental parameters such as the cavity length and so forth.[10] Since k_1' and k_2' are independent of experimental conditions studied at a fixed amount of O_2 and only k_3' varies with C_2H_2 concentration, the transient signal was fitted by a simplified formula by

$$1/t_c - 1/t_0 = C + D\cdot[\exp(-P_1\cdot t) - \exp(-P_2\cdot t)] \quad (2b)$$

where C and D are experimental constants and P_1 (i.e., $k_1'+k_3'$) and P_2 (i.e., k_2') are parameters to be fitted. A typical plot of ($k_1' + k_3'$) versus C_2H_2 concentration, as illustrated in the inset of Figure 1, gives an averaged second-order rate constant k_3 from its slope according to the equation $k_3' = k_0 + k_3[C_2H_2]_0$, where k_0 is the radical decay constant in the absence of the molecular reactant due to the loss of the radical by diffusion away from the probing beam and the decay of probing molecule/radical including k_2'. Its values were typically 2−4 × 10^3 s^{-1} under our experimental conditions. The conditions employed and the results are summarized in Table 1. The Arrhenius plot of the rate constants for the 2-$C_{10}H_7$ + C_2H_2 reaction is shown in Figure 2 for the comparison with that of C_6H_5 + C_2H_2[25] as well as with the theoretically predicted value for the 1-$C_{10}H_7$ + C_2H_2 reaction.[4,6,7] The result shows that the measured reaction rate is about a factor of 5−20 higher than those previously estimated for the 1-$C_{10}H_7$ + C_2H_2 reaction at room temperature, but they are close to each other at higher temperature. Interestingly, within the large scatter of the result, both naphthyl and phenyl appear to have a similar reactivity toward acetylene as that estimated by Wang and Flenklach,[6] where the high pressure limit reaction rates for C_2H_2 addition to phenyl and 1-naphthyl radicals were not affected by the aromatic radical size. A least-squares analysis of the data by convoluting the errors shown in

TABLE 1: Measured Bimolecular Rate Constants (k; 10^{10} cm^3 mol^{-1} s^{-1}) for the 2-$C_{10}H_7$ Reaction with C_2H_2 and Experimental Conditions Studied

T (K)	$[O_2]$ (Torr)	$[C_2H_2]$ (Torr)	k (2-$C_{10}H_7$ + C_2H_2)
303	0.16	0−0.79	2.38 ± 1.56
313	0.08	0−0.94	2.26 ± 1.01
324	0.16	0−0.79	2.93 ± 1.50
333	0.08	0−1.10	2.79 ± 2.52
351	0.16	0−0.94	3.24 ± 0.48
368	0.16	0−1.02	3.93 ± 1.73
393	0.08	0−1.10	3.88 ± 2.08
407	0.16	0−0.79	4.19 ± 1.05
423	0.16	0−0.79	5.30 ± 2.85
448	0.16	0−0.87	5.50 ± 2.19

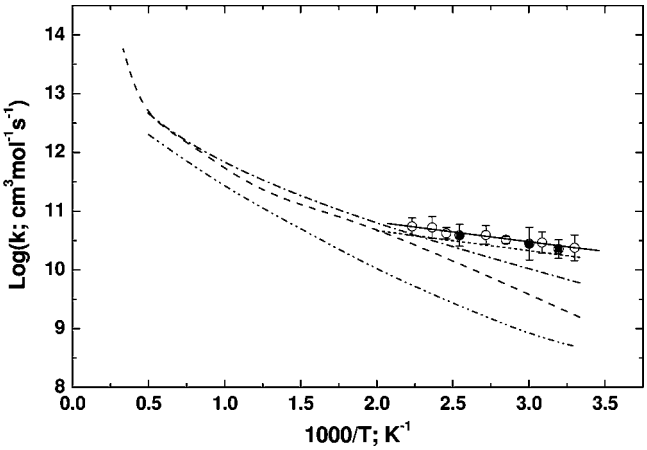

Figure 2. The Arrhenius plot of the rate constants for the 2-$C_{10}H_7$ + C_2H_2 reaction with a fixed amount of O_2 (○, $[O_2] = 0.16$ Torr; ●, $[O_2] = 0.08$ Torr) for comparison with that of the C_6H_5 + C_2H_2 reaction (dotted line, ref 25) and the theoretically predicted values for the 1-$C_{10}H_7$ + C_2H_2 reaction (dashed, ref 4; dash−dotted, ref 7; dash−dot−dotted, ref 6).

the figure gives the first experimentally measured rate constant for 2-$C_{10}H_7$ + C_2H_2

$$k_3 = (3.36 \pm 0.63) \times 10^{11} \times \exp[-(817 \pm 34)/T]\ \mathrm{cm^3\ mol^{-1}\ s^{-1}}$$

in the temperature range of 303−448 K at a total pressure of 40 Torr with the Ar carrier gas.

As shown in the inset of Figure 1, the $k_1' + k_3'$ value, which is sensitive to the fast competitive k_1' for the slow reaction such as $C_{10}H_7$ + C_2H_2, has a relatively large scatter in the measured results. In order to provide a sufficient peroxy radical for detection without removing too much naphthyl for its reaction with C_2H_2, effort is required to optimize the experimental condition for CRDS measurements. The results presented in Figure 2 obtained by employing 0.08 and 0.16 Torr O_2 are in good agreement. Undoubtedly, the direct CRDS detection of the naphthyl, as in the phenyl radical case, should help reduce the large experimental errors and also help broaden our ability to study many more relevant reactions as well. Effort is underway to characterize the spectroscopy of $C_{10}H_7$ radicals by CRDS using a pulsed beam system.

2. Potential Energy Surfaces. The potential energy diagrams obtained at the G2MS//B3LYP/6-311+G(d, p) level of theory are presented in Figure 3. The geometric parameters, vibrational frequencies, and moments of inertia for all of the species predicted by B3LYP/6-311+G(d, p) are summarized in the Supporting Information. Figure 3 includes two reaction systems, 1-$C_{10}H_7$ + HCCH and 2-$C_{10}H_7$ + HCCH. The energy of 2-$C_{10}H_7$ is almost the same as that of 1-$C_{10}H_7$. The transition state (TS0; see Figure 3B) for the 2-$C_{10}H_7$ → 1-$C_{10}H_7$ isomerization is predicted to be 59.8 kcal/mol over 2-$C_{10}H_7$, and the reverse barrier is lower by 0.3 kcal/mol. This implies that the configuration transformation cannot take place readily under the thermal conditions employed.

1-C₁₀H₇ + HCCH. Figure 3A shows that the 1-naphthyl vinyl radical can be formed from the reactants via a-TS1 with a 2.6 kcal/mol barrier and 38.5 kcal/mol of exothermicity. The 1-naphthyl vinyl radical has four isomeric intermediates (or conformers) whose energies are almost the same. The intrinsic reaction coordinate (IRC) analysis confirms that the addition reaction proceeds via a-TS1 to form **a1**. Other isomeric intermediates **a2**, **a3**, and **a4** can be readily formed by terminal C−H bond bending and C−C bond rotational vibrations with <3.5 kcal/mol barriers from **a1**. Following the formation of **a4**, it can continue to undergo dehydrogenation, producing acenaphthylene (**a8**) by two pathways; one takes place via intermediates **a5** and **a7**, while the other via the intermediate **a6**. Evident from the figure, the energy of a-TS7 in the former path is lower than that of a-TS9 in the latter by 9.0 kcal/mol; the latter process is expected to contribute less significantly. From Figure 3A, one can also see that the intermediates **a1** and **a2** can dehydrogenate to give 1-ethynylnaphthalene (**a13**) via transition states a-TS18 and a-TS19, which lie below the reactants by 4.5 and 4.4 kcal/mol, respectively. From the intermediate **a3**, there are three other isomerization subchannels to the intermediates **a9**, **a10**, and **a11** with isomerization barriers of 27.2, 37.6, and 67.1 kcal/mol, respectively. However, because of the high endothermicity and the high barriers for the associated dehydrogenation transition states, the formation of cyclobuta[*a*]naphthalene (**a12**) cannot compete with the production of **a8**. In addition, the hydrogen abstraction reaction from 1-$C_{10}H_7$ + HCCH to $C_{10}H_8$ + CCH is predicted to be endothermic by 19.5 kcal/mol with a loose transition state. Accordingly, for the 1-$C_{10}H_7$ + HCCH reaction, the most favorable reaction channel should be the formation of acenaphthylene (**a8**). This mechanism schematically agrees with the predicted potential energy surface by the other authors.[4−7] A comparison of the stationary points' energies with the values in the literature is shown in Table 2. It can be seen that the maximum difference is within 5 kcal/mol between our predicted value at the G2MS//B3LYP/6-311+G(d, p) level of theory and the one[7] at the G3(MP2,CC)//B3LYP/6-311G(d,p) level of theory. However, the maximum difference is over 10 kcal/mol comparing ours and the values of Wang and Frenklach[6] and Richard et al.[5] with the lower-level AM1 and B3LYP/cc-pVDZ methods, respectively.

2-C₁₀H₇ + HCCH. Similar to the reaction system of 1-$C_{10}H_7$ + HCCH, the addition product (2-naphthyl vinyl radical) in the 2-$C_{10}H_7$ + HCCH reaction is first formed via the transition state b-TS1 with a 2.9 kcal/mol barrier. The **b1** adduct was confirmed to be the addition product according to an IRC analysis. The exothermicity of this process is 39.2 kcal/mol. From Figure 3B, one sees that the adducts **b1**, **b2**, **b3**, and **b4** are the conformers of the 2-naphthyl vinyl radical with almost the same energies. From **b3** and **b4**, the dehydrogenation products cyclobuta[*a*]naphthalene (**b14**=**a12**) and cyclobuta[b]naphthalene (**b11**) can be formed, but the undergoing transition states are over the reactants in energy. From **b1** and **b2**, 2-ethynylnaphthalene (**b13**) can be formed via b-TS19 and b-TS20, which lie below the reactants by 3.4 and 3.6 kcal/mol, respectively. Because the production of $C_{10}H_8$ + CCH, **b11** + H, and **b14** + H is endothermic, the formation of 2-ethynylnaphthalene (**b13**) from **b1** and **b2** is thus expected to be dominant in the 2-$C_{10}H_7$ + HCCH reaction with only 9.6 kcal/mol of exothermicity. In this respect, the 2-$C_{10}H_7$ radical reaction differs distinctly from the 1-$C_{10}H_7$ analogue, which produces **a8** by H-elimination with 38.6 kcal/mol of exothermicity via relatively low lying exit transition states. Its kinetic consequence is discussed below.

3. Predicted Rate Constants. On the basis of the above discussion on both 1- and 2-$C_{10}H_7$ + HCCH, the most favorable reaction pathways are used to calculate rate constants. For 1-$C_{10}H_7$ + HCCH, the reaction pathway is controlled by the addition step, 1-$C_{10}H_7$ + HCCH → a-TS1 → **a1***. The energy-rich adduct **a1** can readily isomerize to other conformers and isomers **a2**, **a3**, **a4**, **a5**, **a6** and **a7** because of the low and

moderate isomerization barriers. Therefore, once the addition reaction occurs, a mixture of these structural isomers as well as the decomposition product (**a8**) is expected to be formed readily. The rate constant of the reaction was predicted with the following simplified reaction pathway

$$1\text{-}C_{10}H_7 + HCCH \rightarrow \text{a-TS1} \rightarrow \mathbf{a1} \rightarrow \text{a-TS6} \rightarrow \mathbf{a5} \rightarrow \text{a-TS7} \rightarrow \mathbf{a7} \rightarrow \text{a-TS8} \rightarrow \mathbf{a8} + H$$

For the $2\text{-}C_{10}H_7$ + HCCH reaction, the reaction may be dominated by the stabilization forming **b1** and the decomposition process

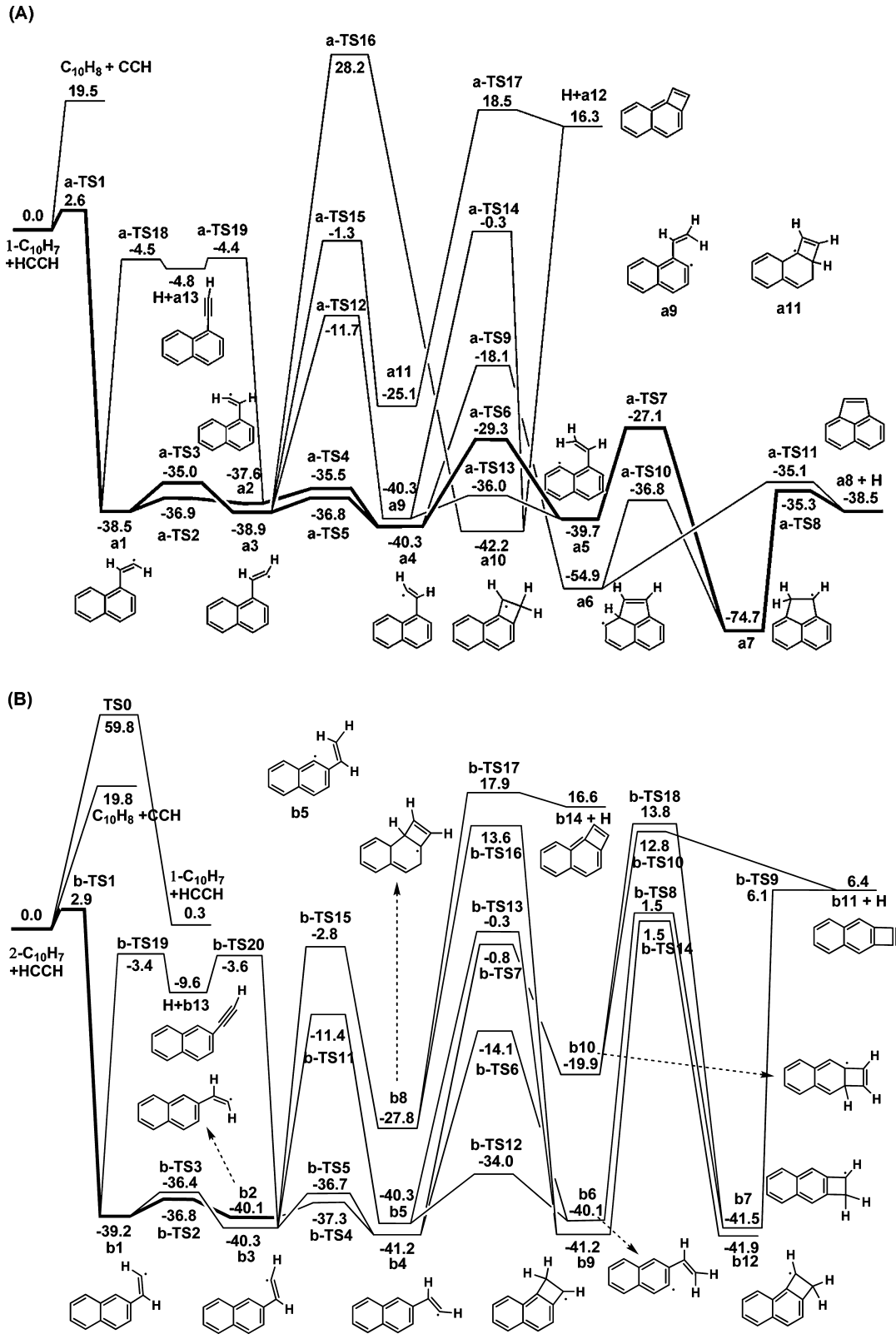

Figure 3. Potential energy surfaces (in kcal/mol) of $1\text{-}C_{10}H_7$ (A) and $2\text{-}C_{10}H_7$ (B) with HCCH at the G2MS level based on the geometric parameters optimized by B3LYP/6-311+G(d,p). The major product channels are marked with bold lines.

$$2\text{-}C_{10}H_7 + HCCH \rightarrow \text{b-TS1} \rightarrow (\mathbf{b1},\mathbf{b2}) \rightarrow (\text{b-TS19}, \text{b-TS20}) \rightarrow \mathbf{b13} + H$$

Similar to the case of the **a1** adduct in $1\text{-}C_{10}H_7$ + HCCH, we may expect the existence of a mixture of **b2**, **b3**, **b4**, **b5**, and **b6** with **b1** through the collisional stabilization process.

Because the C−C torsional frequencies of **a1**, a-TS1, **b1**, and b-TS1 are predicted to be 78, 33, 20, and 15 cm^{-1}, respectively, in the rate constant calculation, the first vibrational mode (78 cm^{-1}) is treated as hindered rotation with a force constant of 1.236 cm^{-1} and a rotation barrier of 630 cm^{-1}, while the vibration modes of the latter three species are treated as free rotations with rotational constants of 1.047, 1.457, and 1.140 cm^{-1}, respectively.

Figure 4 displays the predicted rate constants of the $1\text{-}C_{10}H_7$ + HCCH reaction as a function of temperature in the 200−1000 K range. The stabilization rate constant for **a1**, k(**a1**), is strongly pressure-dependent, with negative temperature dependence at 1−760 Torr pressures due to competition with its decomposition reaction producing **a8** + H. At 10 atm, k(**a1**) increases with T at 200−400 K, reflecting the 2.6 kcal/mol addition barrier, and decreases rapidly with T above 400 K, attributable to the decrease in the collisional deactivation efficiency as well as to the increase in the decomposition rate. Conversely, k(**a8**+H) appears to have a weak negative pressure dependence due to the low exit barriers and a strong positive temperature dependence which reflects the addition barrier. Combining Figure 4A and B, one can see that the dominant rate constant is k(**a8**+H), and only at low temperatures and over 10 atm, k(**a1**) becomes a major component. Comparing with the theoretical high-pressure-limit rate constants by Richter et al.[5] and Kislov et al.,[7] our predicted values are about 2.2 and 2.5 times greater than theirs, respectively, at 1000 K. However, Wang's result[6] at 300 K is smaller than ours by 56 times because of the semiempirical quantum chemical method employed.

Figure 5 illustrates the predicted total and branching rate constants of the $2\text{-}C_{10}H_7$ + HCCH reaction in the 200−1000 K range. Contrary to k(**a1**), k(**b1**) exhibits no pressure dependence under 500 K even at 1 Torr pressure because of the absence of a competitive decomposition process. The pressure effect appears only at T > 500 K, attributable to the decrease in collisional deactivation and the appearance of competitive decomposition processes including the back reaction. The k(**b1**) has a positive temperature dependence below about 600 K, reflecting the entrance 2.9 kcal/mol barrier; but it has a negative temperature dependence over 600 K due to the appearance of decomposition processes including the back reaction and **b13** production as manifested by the values of k(**b13**+H) shown in Figure 5 B. It is apparent that k(**b1**) accounts for the major component of the rate constant at T < 600 K, while k(**b13**+H) becomes competitive at T > 700 K.

TABLE 2: Comparison of the Stationary Point Energies with the Values of Previous Works (in units of kcal/mol)

species	this work	Wang et al.[6]	Richard et al.[5]	Kislov et al.[7]
$1\text{-}C_{10}H_7$ + HCCH	0.0	0.0	0.0	0.0
a4	−40.3	−36.2	−39.1	−39.6
a5	−39.7	−45.1 ± 5.0	−29.2	
a6	−54.9		−59.7	−59.2
a7	−74.4		−83.1	
a8 + H	−38.5	−34.9	−37.5	−40.0
a9	−40.3		−38.4	
a10	−42.2		−53.5	
a11	−25.1		−33.6	
a12 + H	16.3		14.9	
a13 + H	−4.8	−7.0	−10.4	
a-TS1	2.6	4.3		2.3
a-TS9	−18.1	−24.2 to −4.2		−23.0
a-TS11	−35.1	−23.5		−32.9
a-TS18	−4.5	−5.0		

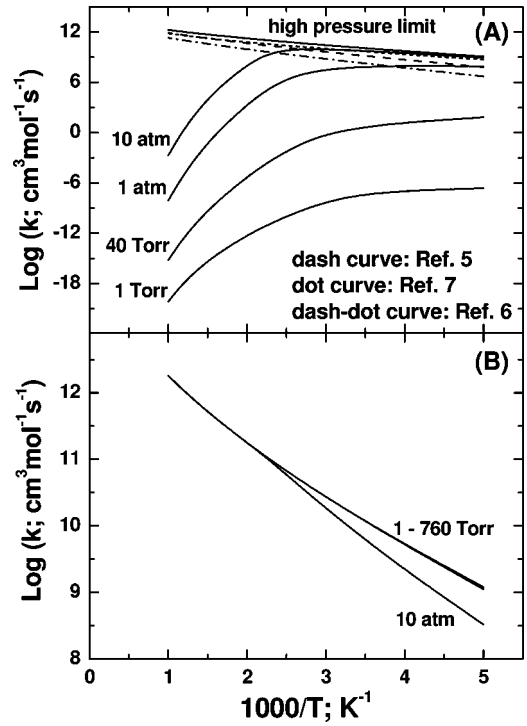

Figure 4. Predicted rate constants of the $1\text{-}C_{10}H_7$ + HCCH → **a1** (A) and **a8** + **H** (B) reactions as a function of temperature at 200−1000 K.

For modeling applications, the predicted rate constants are fitted to modified Arrhenius expressions with three parameters as presented in Table 3.

4. Kinetic Modeling. On the basis of our predicted bond dissociation energy of $2\text{-}C_{10}H_7$−Br at the G2MS level of theory, 84.0 kcal/mol, the $2\text{-}C_{10}H_7$ produced by the photodissociation reaction at 193 nm may possess ≤64 kcal/mol of internal energy, which is only 4.2 kcal/mol above the barrier for the 2 → 1 isomerization reaction. Thus, one expects that the $2\text{-}C_{10}H_7$ radical can be rapidly thermalized during the course of the addition reaction. In order to confirm the validity of eq 2a employed for kinetic analysis, we have carried out kinetic modeling for the time-resolved $C_{10}H_7O_2$ concentration profiles with the SENKIN program[26] using a set of reactions given in Table 4 to simulate the kinetics for the $2\text{-}C_{10}H_7 + C_2H_2$ reaction with an added fixed concentration of O_2 at 303 and 407 K. All reactions used for the modeling were based on our theoretically predicted rate constants (given in Table 4) for the primary reactions, with assumed values for secondary processes. Since the modeled results were given as mole fractions, they were scaled and normalized at 50 μs for comparison with time-resolved experimental CRDS signals and their fitted profiles in Figure 6. The solid curves presented in the figure represent the modeled results using the mechanism and the rate constants listed in Table 4, and the dashed curves are the fitted values using eq 2b. As shown in the figure, both profiles agree closely to each other.

We also examined any other possible contributions in the observed $C_{10}H_7O_2$ profiles such as $1\text{-}C_{10}H_7O_2$ and $C_{10}H_7C_2H_2O_2$. Since the $C_{10}H_7C_2H_2O_2$ product could be formed by the $C_{10}H_7C_2H_2 + O_2$ reaction, which is similar to our earlier work for the $C_6H_5C_2H_2 + O_2$ reaction, we would expect $C_{10}H_7C_2H_2O_2$

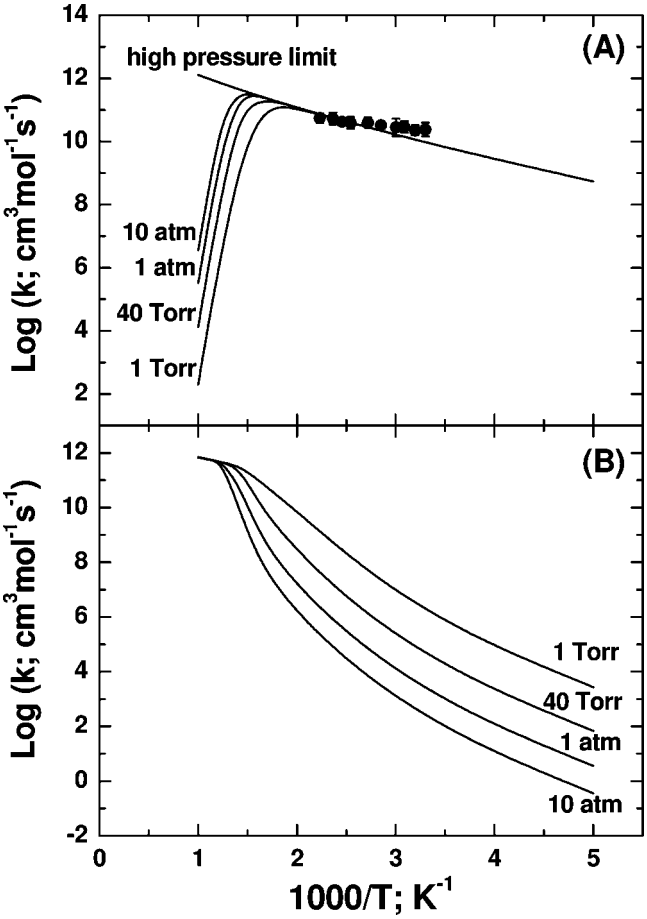

Figure 5. Predicted rate constants of the 2-$C_{10}H_7$ + HCCH → **b1** (A) and **b13** + **H** (B) reactions as a function of temperature at 200−1000 K. Solid circle: experimental data at 40 Torr.

TABLE 3: Predicted Rate Constant Expressions of the 1- and 2-$C_{10}H_7$ + C_2H_2 Reactions ($k = A \cdot T^n \cdot \exp(C/T)$ in units of cm³ mol⁻¹ s⁻¹)

reaction	pressure	T (K)	A	n	C
1-$C_{10}H_7$ + C_2H_2 → **a1**	40 Torr	200−1000	6.55×10^{133}	−48.41	−9418
	1 atm	200−1000	5.53×10^{181}	−61.14	−15362
	10 atm	200−400	1.60×10^{36}	−8.70	−3348
		400−1000	2.20×10^{185}	−60.25	−17018
	high P	200−1000	2.84×10^{7}	1.77	−1128
1-$C_{10}H_7$ + C_2H_2 → **a8** + H	40 Torr	200−1000	2.84×10^{7}	1.77	−1128
	1 atm	200−1000	5.60×10^{7}	1.68	−1178
	10 atm	200−1000	1.17×10^{11}	0.67	−1900
2-$C_{10}H_7$ + C_2H_2 → **b1**	40 Torr	200−600	5.38×10^{7}	1.65	−1289
		600−1000	3.47×10^{464}	−141.62	−82287
	1 atm	200−700	6.60×10^{8}	1.28	−402
		700−1000	1.11×10^{355}	−108.24	−57225
	10 atm	200−700	4.37×10^{7}	1.68	−1281
		700−1000	1.59×10^{574}	−172.50	−115646
	High-P	200−1000	8.60×10^{7}	1.58	−1314
2-$C_{10}H_7$ + C_2H_2 → **b13** + H	40 Torr	200−700	5.33×10^{-52}	21.65	1522
		700−1000	2.90×10^{42}	−8.83	−9562
	1 atm	200−800	2.22×10^{-64}	25.45	2640
		800−1000	8.26×10^{15}	−0.996	−2505
	10 atm	200−800	8.54×10^{-79}	30.00	4052
		800−1000	5.92×10^{39}	−7.99	−9132

also has the similar absorption in the same region as most π-complexed peroxy radicals, like $C_2H_3O_2$,[27] $C_6H_5O_2$,[28] $C_6H_5C_2H_2O_2$,[29] and $C_{10}H_7O_2$,[8] exhibit strong continuous broad absorptions in the 400−700 nm region. According to our sensitivity analysis and the concentration profiles as shown in Figure 7, however, the concentrations of $C_{10}H_7C_2H_2O_2$ and 1-$C_{10}H_7$ radicals are too small to have any effects on the observed $C_{10}H_7O_2$ profiles. In the figure, some concentration profiles were enlarged for clarity and better comparison.

TABLE 4: Rate Constants[a] for the Kinetic Modeling of the 2-$C_{10}H_7$ + C_2H_2 Reaction

reactions	A	n	E_a	ref
2-$C_{10}H_7$ = 1-$C_{10}H_7$	2.16×10^{7}	0.0	44180	this work
1-$C_{10}H_7$ = 2-$C_{10}H_7$	1.51×10^{7}	0.0	44180	this work
1-$C_{10}H_7$ + C_2H_2 = 1-$C_{10}H_7C_2H_2$	2.81×10^{7}	1.77	2240	this work
2-$C_{10}H_7$ + C_2H_2 = 2-$C_{10}H_7C_2H_2$	5.38×10^{7}	1.65	2560	this work
1-$C_{10}H_7$ + 1-$C_{10}H_7$ = $C_{20}H_{14}$	1.00×10^{13}	0.0	0	*b*
1-$C_{10}H_7$ + 2-$C_{10}H_7$ = $C_{20}H_{14}$	1.00×10^{13}	0.0	0	*b*
2-$C_{10}H_7$ + 2-$C_{10}H_7$ = $C_{20}H_{14}$	1.00×10^{13}	0.0	0	*b*
1-Np + O_2 = $C_{10}H_7O_2$	1.53×10^{12}	0.0	−900	8
2-Np + O_2 = $C_{10}H_7O_2$	1.53×10^{12}	0.0	−900	8
$C_{10}H_7O_2$ = others	3.00×10^{3}	0.0	0	*c*
1-$C_{10}H_7C_2H_2$ + O_2 = $C_{10}H_7C_2H_2O_2$	3.20×10^{11}	0.0	−1510	*d*
2-$C_{10}H_7C_2H_2$ + O_2 = $C_{10}H_7C_2H_2O_2$	3.20×10^{11}	0.0	−1510	*d*
$C_{10}H_7C_2H_2O_2$ = $C_{10}H_7CHO$ + HCO	1.68×10^{3}	0.0	0	*d*

[a] Rate constants, defined by $k = AT^n \exp(-E_a/RT)$, are given in units of cm³, mole, and s; E_a is in units of cal/mol. [b] Estimated. [c] The reaction rate varied in the range of $2-4 \times 10^3$ s^{-1} at each signal. [d] Estimated from the $C_6H_5C_2H_2$ + O_2 reaction (ref 29).

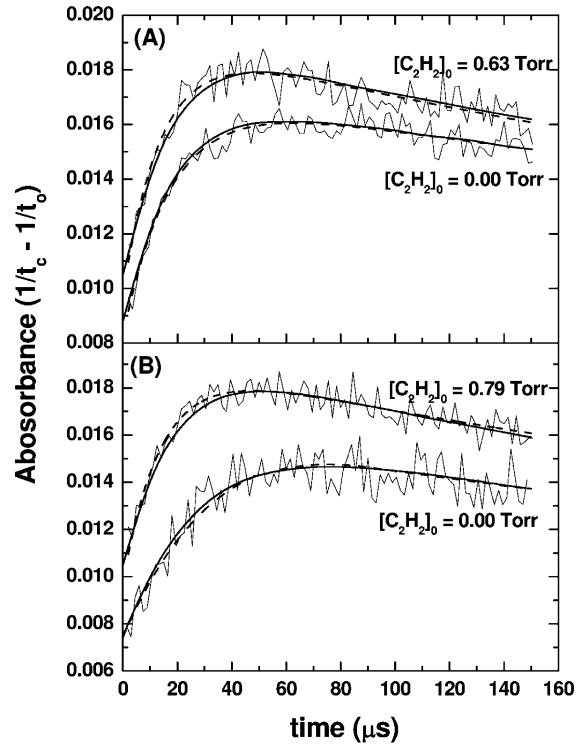

Figure 6. Typical time-resolved absorption plots of $C_{10}H_7O_2$ formed in the 2-$C_{10}H_7$ + C_2H_2 reaction at 303 (A) and 407 K (B) with a fixed concentration of $[O_2] = 0.16$ Torr and initial concentration of [2-$C_{10}H_7$] = 0.01 Torr; solid curves are kinetically modeled results, and dashed curves are fitted values using eq 2.

Conclusion

The total rate constant for the $C_{10}H_7$ + C_2H_2 reaction has been investigated in the temperature range of 303−448 K by monitoring the $C_{10}H_7O_2$ radical in the visible region by cavity ringdown spectrometry (CRDS) using the 2-$C_{10}H_7Br$ as a radical source by photolysis at 193 nm in the presence of added O_2 in a small fixed concentration. The kinetics was determined by monitoring the change in the $C_{10}H_7O_2$ yields (or signals) as a function of the concentration of C_2H_2, using two different

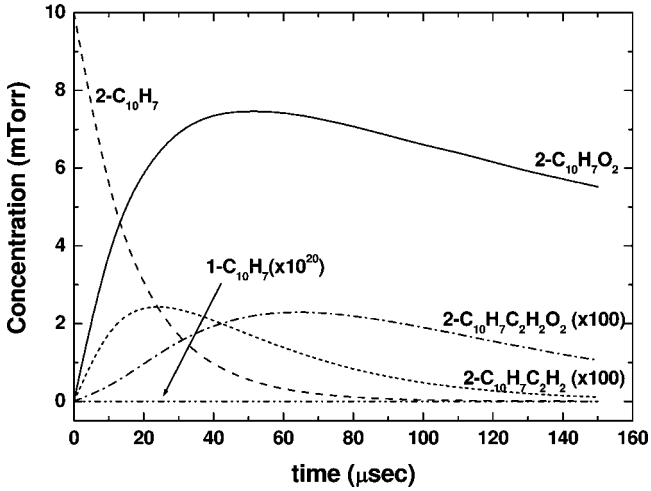

Figure 7. Modeled concentration profiles for the reactant and products in the 2-$C_{10}H_7$ + C_2H_2 reaction at 303 K with fixed concentrations of $[O_2]$ = 0.16 Torr, $[2\text{-}C_{10}H_7]_0$ = 0.01 Torr, and $[C_2H_2]_0$ = 0.63 Torr.

mixtures containing the radical precursor and small fixed amounts of O_2. The measured rate constant for 2-$C_{10}H_7$ + C_2H_2 can be presented by $k = (3.36 \pm 0.63) \times 10^{11} \exp[-(817 \pm 34)/T]$ cm^3 mol^{-1} s^{-1} in the temperature range of 303−448 K at a total pressure of 40 Torr Ar, effectively reaching its high-pressure limit.

Additionally, the potential energy surfaces, calculated by G2MS//b3LYP/6-311+G(d,p), show that the reactions of 1- and 2-$C_{10}H_7$ with C_2H_2 occur first by addition forming the excited naphthyl vinyl radicals, which can undergo isomerization to various structural isomers or elimination of a hydrogen atom by low-barrier decomposition channels. The mechanisms for the decomposition of the two radicals were predicted to be significantly different under experimental conditions; the excited 1-$C_{10}H_7C_2H_2$ radical produces predominantly acenaphthylene due to its low formation barrier, while the excited 2-$C_{10}H_7C_2H_2$ radical can be effectively stabilized by collisional deactivation because of its high exit barrier. The predicted rate constant for the 2-$C_{10}H_7$ reaction is in reasonable agreement with the experimental values under the conditions employed.

The preliminary kinetic data presented above have a significantly large scatter because of the indirect monitoring of the naphthyl peroxyl radical. It is believed that the direct detection of the naphthyl radical by CRDS, as in the case of C_6H_5 demonstrated in our earlier studies, should greatly improve the accuracy of kinetic data. Within the limit of the detection error, the reactivities of the 2-naphthyl and phenyl radicals toward acetylene were found to be similar. An experiment is underway to search for detectable CRDS transitions of 1- and 2-naphthyl radicals for improved kinetic measurements.

Acknowledgment. The authors are grateful for the partial support of this work from the Basic Energy Sciences, Department of Energy, under Contract No. DE-FG02-97-ER14784. We also thank the Cherry L. Emerson Center of Emory University for the use of its resources and for its support to H.M.T.N. as a visiting fellow.

Supporting Information Available: Geometric parameters, frequencies, energies, and moments of inertia optimized by B3LYP/6-31+G(d,p), as well as the energies corrected by G2MS. This material is available free of charge via the Internet at http://pubs.acs.org.

References and Notes

(1) Frenklach, M.; Wang, H. *Proc. Combust. Inst.* **1991**, *23*, 1559.
(2) Frenklach, M. *Phys. Chem. Chem. Phys.* **2002**, *4*, 2028–2037.
(3) Tokmakov, I. V.; Lin, M. C. *J. Am. Chem. Soc.* **2003**, *125*, 11397–11408.
(4) Richter, H.; Benish, T. G.; Mazyar, O. A.; Green, W. H.; Howard, J. B. *Proc. Combust. Inst.* **2000**, *28*, 2609.
(5) Richter, H.; Mazyar, O. A.; Sumathi, R.; Green, W. H.; Howard, J. B.; Bozzelli, J. W. *J. Phys. Chem. A* **2001**, *105*, 1561.
(6) Wang, H.; Frenklach, H. *J. Phys. Chem.* **1994**, *98*, 11465–11489.
(7) Kislov, V. V.; Islamova, N. I.; Kolker, A. M.; Lin, S. H.; Mebel, A. M. *J. Chem. Theory Comput.* **2005**, *1*, 908–924.
(8) Park, J.; Xu, Z. F.; Lin, M. C. *J. Phys. Chem. A* **2009**, *113*, 5348–5354.
(9) Yu, T.; Lin, M. C. *J. Phys. Chem.* **1994**, *98*, 9697.
(10) (a) Yu, T.; Lin, M. C. *J. Am. Chem. Soc.* **1993**, *115*, 4371. (b) Lin, M. C.; Yu, T. *Int. J. Chem. Kinet.* **1993**, *25*, 875. (c) Park, J.; Lin, M. C. American Chemical Society Special Publication Series on Cavity Ringdown Spectroscopy; American Chemical Society: Washington, DC, 1999; Chapter 13, p 196.
(11) Gonzalez, C.; Schlegel, H. B. *J. Chem. Phys.* **1989**, *90*, 2154.
(12) Gonzalez, C.; Schlegel, H. B. *J. Phys. Chem.* **1990**, *94*, 5523.
(13) (a) Becke, A. D. *J. Chem. Phys.* **1993**, *98*, 5648. (b) Becke, A. D. *J. Chem. Phys.* **1992**, *96*, 2155.
(14) Lee, C.; Yang, W.; Parr, R. G. *Phys. Rev. B* **1988**, *37*, 785.
(15) Froese, R. D. J.; Humbel, S.; Svensson, M.; Morokuma, K. *J. Phys. Chem. A* **1997**, *101*, 227.
(16) Frisch, M. J.; Trucks, G. W.; Schlegel, H. B.; Scuseria, G. E.; Robb, M. A.; Cheeseman, J. R.; Montgomery, J. A., Jr.; Vreven, T.; Kudin, K. N.; Burant, J. C.; Millam, J. M.; Iyengar, S. S.; Tomasi, J.; Barone, V.; Mennucci, B.; Cossi, M.; Scalmani, G.; Rega, N.; Petersson, G. A.; Nakatsuji, H.; Hada, M.; Ehara, M.; Toyota, K.; Fukuda, R.; Hasegawa, J.; Ishida, M.; Nakajima, T.; Honda, Y.; Kitao, O.; Nakai, H.; Klene, M.; Li, X.; Knox, J. E.; Hratchian, H. P.; Cross, J. B.; Bakken, V.; Adamo, C.; Jaramillo, J.; Gomperts, R.; Stratmann, R. E.; Yazyev, O.; Austin, A. J.; Cammi, R.; Pomelli, C.; Ochterski, J. W.; Ayala, P. Y.; Morokuma, K.; Voth, G. A.; Salvador, P.; Dannenberg, J. J.; Zakrzewski, V. G.; Dapprich, S.; Daniels, A. D.; Strain, M. C.; Farkas, O.; Malick, D. K.; Rabuck, A. D.; Raghavachari, K.; Foresman, J. B.; Ortiz, J. V.; Cui, Q.; Baboul, A. G.; Clifford, S.; Cioslowski, J.; Stefanov, B. B.; Liu, G.; Liashenko, A.; Piskorz, P.; Komaromi, I.; Martin, R. L.; Fox, D. J.; Keith, T.; Al-Laham, M. A.; Peng, C. Y.; Nanayakkara, A.; Challacombe, M.; Gill, P. M. W.; Johnson, B.; Chen, W.; Wong, M. W.; Gonzalez, C.; Pople, J. A. *Gaussian 03*, revision B.03; Gaussian, Inc.: Pittsburgh, PA, 2003.
(17) Wardlaw, D. M.; Marcus, R. A. *Chem. Phys. Lett.* **1984**, *110*, 230.
(18) Wardlaw, D. M.; Marcus, R. A. *J. Chem. Phys.* **1985**, *83*, 3462.
(19) Klippenstein, S. J. *J. Chem. Phys.* **1992**, *96*, 367.
(20) Klippenstein, S. J.; Marcus, R. A. *J. Chem. Phys.* **1987**, *87*, 3410.
(21) Klippenstein, S. J.; Wagner, A. F.; Dunbar, R. C.; Wardlaw, D. M.; Robertson, S. H. *VARIFLEX*, version 1.00; 1999.
(22) Hippler, H.; Troe, J.; Wendelken, H. J. *J. Chem. Phys.* **1983**, *78*, 6709.
(23) Lide, D. R. *CRC Handbook Chemistry and Physics*, 71st ed.; CRC Press: Boca Raton, FL, 1990; pp 6−49.
(24) Rabinovitch, B. S.; Tardy, D. C. *J. Chem. Phys.* **1966**, *45*, 3720.
(25) Yu, T.; Lin, M. C.; Melius, C. F. *Int. J. Chem. Kinet.* **1994**, *26*, 1095.
(26) Lutz, A. E.; Kee, R. J.; Miller, J. A. *SENKIN: A FORTRAN Program for Predicting Homogeneous Gas-Phase Chemical Kinetics with Sensitivity Analysis*; Report No. SAND87-8248; Sandia National Laboratories: Livermore, CA, 1988.
(27) (a) Mertens, R.; von Sonntag, C. *Angew. Chem., Int. Ed. Engl.* **1994**, *33*, 1262–1264. (b) Fang, X.; Mertens, R.; von Sonntag, C. *J. Chem. Soc., Perkin Trans. 2* **1995**, *6*, 1033–1036. (c) Thorn, R. P.; Payne, W. A.; Stief, L. J. *J. Phys. Chem.* **1996**, *100*, 13594–13602.
(28) Yu, T.; Lin, M. C. *J. Am. Chem. Soc.* **1994**, *116*, 9571.
(29) Park, J.; Lin, M. C. *Proc. Combust. Inst.* **2009**, *32*, 305–310.

JP905854C